Role of refractive index mismatch in backward nonlinear optical imaging

Jarno N. van der Kolk[1,*], Charalambos Kioulos[1], Antonino Calà Lesina[1], Stéphane Bancelin[2], François Légaré[2], and Lora Ramunno[1,†]

[1]*Department of Physics and Centre for Research in Photonics, University of Ottawa, Ottawa, ON, K1N 6N5, Canada.* [2]*Institut National de la Recherche Scientifique – Centre Énergie, Matériaux et Télécommunication, Varennes, QC, J3X 1S2, Canada*

[*]*jvanderk@uottawa.ca,* [†]*Lora.Ramunno@uottawa.ca*

Abstract: Epi nonlinear optical imaging is used to image subresolution features. We find a refractive index mismatch between background medium and object affects imaging significantly. We study second harmonic generation microscopy of collagen fibrils as example.
© 2018 The Author(s)
OCIS codes: (180.4315) Nonlinear microscopy; (190.2620) Harmonic generation and mixing.

Epi-collected signals for coherent nonlinear imaging techniques contain valuable information. Generally, the radiation in the epi direction is much weaker than that in the forward direction because the phase matching conditions promote coherent addition in the forward but destructive interference in the backward direction. However, short coherence length also makes the epi-signal particularly sensitive to the thickness of the structure, thus it is uniquely suited to obtain sub-resolution structural information. For coherent anti-Stokes Raman scattering (CARS), the epi-signal contains structural information about lipid droplets in the order of 0.3λ, where λ is the wavelength of the CARS signal, while forward CARS is only sensitive to the larger structures [1–3]. With third harmonic generation (THG), epi-THG can be of comparable strength to forward THG for nanostructures and thin films [4–6]. For second harmonic generation (SHG) imaging of collagen fibrils, it has been shown that ratio of the forward SHG intensity signal to that in the backward provides information about the diameters of the fibrils down to 85 nm even though the wavelength of the SHG radiation is 405 nm [7].

Here, we consider SHG imaging of collagen fibrils which can be found in a wide array of biological tissues such as bones, tendons, arteries, cornea and many others. They form the basis for more complex hierarchies such as collagen fibres which in turn can comprise tendons and bone [8, 9]. The fibrils are involved in most of the mechanical properties, such as elasticity and compressibility [10]. Additionally, some pathologies are traced down to failures in the structure created by fibrils. Diseases such as Osteoarthritis, which leads to joint pain, show changes in the structure of the collagen tissue and cartilage degradation as one of the earliest symptoms [11]. SHG is a non-linear optical process that is particularly strong in collagen fibrils due to the chiral structure of the collagen molecules and the highly organized hierarchical structures, which enables label-free imaging of collagen tissue [12]. The fibrils are smaller than the diffraction limit at the commonly used infrared frequencies, but it has been shown that the radiation pattern of the SHG signal correlates with both the size and distribution of subwavelength-sized scatterers because of the coherent nature of SHG [13]. In particular, the ratio of the far-field SHG intensity in the forward direction to that in the backward, *i.e.* the F/B ratio, is a metric that is often used. Through numerical modelling, properties such as fibril diameter and fibril bundling are obtained quantitatively from the F/B ratio [14–16] and images of the F/B ratio map out the distribution of fibril size in cartilage and bone [7].

However, the above models do not take into account inhomogeneity of the linear index of refraction. Our calculations show that small differences of the refractive index of $\Delta n/n \approx 0.1$ between the collagen fibrils and the background medium, as commonly found in biological tissue and prepared samples, can lead to a significant change in the measured F/B ratio of a distribution of fibrils in mouse and rat tail tendon. We find decreases of up to 25 % occur between fibrils embedded in a $n = 1.47$ background medium versus those in $n = 1.33$ due to near-field enhancements of the pump occurring inside the fibrils in the order of a few percent. While we find that this does not significantly affect the far-field signal in the forward direction, the far-field signal in the backward direction is particularly sensitive as these enhancements alter phase matching conditions.

We model single collagen fibrils as dielectric cylinders in various dielectric media, illuminated by a plane wave. When the medium has the same refractive index as the cylinder, *i.e.* $\Delta n = 0$, analytical expressions for the forward and

backward far-field SHG signal are [12]:

$$I_{\text{forward}} \propto k^4 r^4 \qquad I_{\text{backward}} \propto k^2 r^2 J_1(2kr)^2, \tag{1}$$

where k is the wave number of the SHG radiation, r is the radius of the cylinder, and J_1 is the Bessel function of the first kind. The signal in the forward direction scales to the fourth power of the cylinder radius because the generated SHG signal for each scatterer within the fibril cylinder is always phase-matched. The backward signal on the other hand is not; it will destructively interfere with the other scatterers in the cylinder as expressed by the zeros of the Bessel function. In that case the F/B ratio becomes very large.

For a fibril cylinder with a refractive index that is different from the background medium ($\Delta n \neq 0$), we apply Mie theory for electromagnetic scattering by a cylinder to calculate the electric fields of the input beam [17]. Then we obtain the induced nonlinear polarization within the cylinder ($P \propto E^2$) and from this calculate the far-field SHG signal using a free-space Green's function approach.

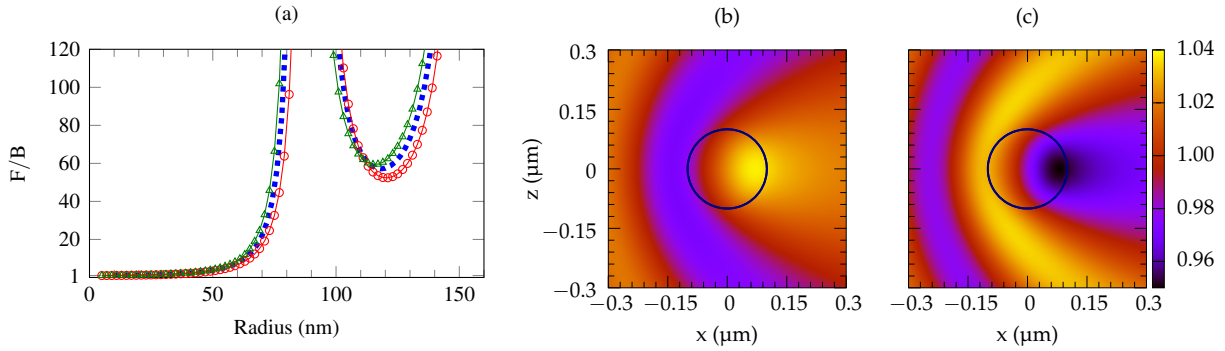


Fig. 1: The forward-to-backward ratio of a single cylinder is shown in (a) for a dielectric background medium of $n = 1.33$ (red circles), $n = 1.40$ (blue squares), and $n = 1.47$ (green triangles). The near-field of the input beam at 810 nm for a single $r = 100$ nm fibril is shown for $n = 1.33$ in (b) and $n = 1.47$ in (c).

We compare $\Delta n = 0$ and $\Delta n \neq 0$ by plotting the F/B ratios versus fibril radius for a $\lambda = 810$ nm plane wave as shown in Fig. 1a. The fibril always has $n = 1.40$ and is embedded in a background medium with $n = 1.33$ (red circles), $n = 1.40$ (blue squares), or $n = 1.47$ (green triangles). For small radii, the difference between Eqs. (1) and the Mie/Green's function calculations is very small as expected, but for fibrils larger than 70 nm, the deviation becomes noticeable. For example, a cylinder in the $n = 1.33$ medium with a radius of 83 nm has an F/B ratio that is 3.2 times smaller than the index-matched case. Fibrils in biological tissues generally have a radius smaller than 100 nm, however in rat and mouse tail tendon larger ones do occur in small numbers [18, 19].

The difference between F/B ratios from $\Delta n = 0$ and $\Delta n \neq 0$ is due to the enhanced electric fields of the pump beam. In Figs. 1b and 1c, we plot those fields in and around a cylinder with a radius of $r = 100$ nm for two different background dielectric media. Regions of enhanced and decreased field strengths up to 5 % within the cylinder are clearly visible. However, the average field strength inside of a cylinder in a $n = 1.33$ medium only increases by 1.3 % whereas the average field inside of a cylinder in a $n = 1.47$ medium decreases by just 0.9 %. In the forward direction, where the SHG signal is added coherently, only the average field matters and thus has little effect. However, in the backward direction destructive interference conditions of the SHG radiation are sensitive to small changes of the field anywhere in the cylinder. This is responsible for the distortion of the peaks in figure 1a. Near where complete destructive interference takes place, *i.e.* when the denominator in the F/B ratio is close to zero, the effect is substantial. It is not the overall change in field strength that causes the F/B ratio to be affected; it is an altered destructive interference effect.

Next we determine the effect on collagen tissue, where collagen fibrils have a distribution of radii, located at random positions. Multiple fibrils exist in the focal volume and a fraction f of those are aligned in the opposite direction to the other fibrils. We consider mouse tail tendon, where even though a majority of the fibrils have a radius smaller than 75 nm, fibrils larger than 100 nm do occur [19]. We randomly place the fibrils in a non-overlapping tightly-packed configuration and assign each fibril randomly either a positive (with probability f) or negative $\chi^{(2)}$, which is consistent with samples found in nature. The sample has a cross sectional area of $1.1 \times 4.5\,\mu$m which is consistent with the focus of a tightly-focused beam. The sample is illuminated by a plane wave with $\lambda = 810$ nm and the SHG signal is collected in the far-field. This is repeated 100,000 times for randomly generated samples for both a background medium of $n = 1.33$ as well as $n = 1.47$. We find that the ratio of the average intensity in the forward direction to that

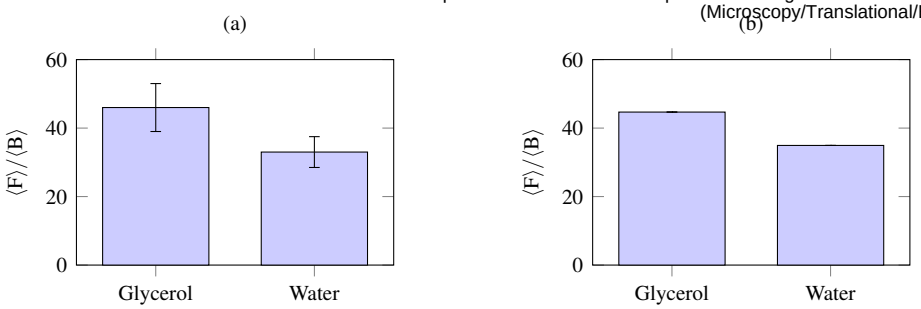


Fig. 2: Experimental F/B measurements for mature mouse tail tendon in glycerol and water are shown in (a). Theoretical F/B ratios for simulated fibrillar tissue with $f = 0.49$ are shown in (b).

in the backward for $n = 1.33$ is decreased by $21.9 \pm 0.4\,\%$ with respect to $n = 1.47$.

We then perform corresponding measurements, comparing the F/B ratio of mouse tail tendon immersed in glycerol and in water. The samples were imaged on a custom-built laser-scanning multiphoton microscope. For a complete description of the setup see [7]. The input laser was tuned to 810 nm and tightly focused on the sample using a water dipping lens (40x, NA 1.15, Olympus). The fibrils in the mouse tail tendon were immersed in either water ($n = 1.33$) or glycerol ($n = 1.47$) such that a refractive index mismatch exists between the fibrils and the background medium. Samples were placed on a glass slide without coverslips on top. The results after five measurements are shown in Fig. 2a. An decrease of $28 \pm 9\,\%$ is observed, agreeing well with theoretical predictions within the error ranges shown in Fig. 2b for $f = 0.49$. For other values of f, the decrease of the F/B of glycerol compared to water remains 21.9 % even though the absolute F/B values are dependent on f.

Our findings show that a small mismatch in the refractive index of $\Delta n/n \approx 0.1$ between object and background medium can have a pronounced impact on backward nonlinear imaging. The F/B ratio for the SHG signal of the collagen fibrils larger than $r = 70\,\text{nm}$ is affected. A Δn also has a pronounced effect on imaging of tissue where a distribution of fibrils is in the focus, such as in mouse tail tendon. This is supported by experimental measurements. Even though the signal from small fibrils will not change significantly, it does for larger fibrils which occur often due to the long tail of the fibril distribution of tissues such as tendon. This may skew diameter measurements such as those in [7] where near-field effects are not taken into account. Therefore consideration to potential refractive index mismatches must be made when interpreting concerning fibril diameters as even small refractive index mismatches can have a significant effect.

References

1. H. Wang, Y. Fu, P. Zickmund, R. Shi, and J.-X. Cheng, Biophysical Journal **89**, 581–591 (2005).
2. I. W. Schie, T. Weeks, G. P. McNerney, S. Fore, J. K. Sampson, S. Wachsmann-Hogiu, J. C. Rutledge, and T. Huser, Optics Express **16**, 2168 (2008).
3. C. Krafft, I. W. Schie, T. Meyer, M. Schmitt, and J. Popp, Chem. Soc. Rev. **45**, 1819–1849 (2016).
4. C.-F. Chang, H.-C. Chen, M.-J. Chen, W.-R. Liu, W.-F. Hsieh, C.-H. Hsu, C.-Y. Chen, F.-H. Chang, C.-H. Yu, and C.-K. Sun, Optics Express **18**, 7397 (2010).
5. D. Sandkuijl, A. E. Tuer, D. Tokarz, J. E. Sipe, and V. Barzda, Journal of the Optical Society of America B **30**, 382 (2013).
6. C. Rodríguez and W. Rudolph, Optics Letters **39**, 6042 (2014).
7. M.-A. Houle, C.-A. Couture, S. Bancelin, J. Van der Kolk, E. Auger, C. Brown, K. Popov, L. Ramunno, and F. Légaré, Journal of Biophotonics **8**, 993–1001 (2015).
8. H. F. Lodish, ed., *Molecular cell biology* (W.H. Freeman, New York, 2000), 4th ed.
9. A. Gautieri, S. Vesentini, A. Redaelli, and M. J. Buehler, Nano Letters **11**, 757–766 (2011).
10. M. A. Meyers, J. McKittrick, and P.-Y. Chen, Science **339**, 773–779 (2013).
11. L. Troeberg and H. Nagase, Biochimica et Biophysica Acta (BBA) - Proteins and Proteomics **1824**, 133–145 (2012).
12. I. Freund, M. Deutsch, and A. Sprecher, Biophysical Journal **50**, 693–712 (1986).
13. J. Mertz and L. Moreaux, Optics Communications **196**, 325 – 330 (2001).
14. C. P. Brown, M.-A. Houle, K. Popov, M. Nicklaus, C.-A. Couture, M. Laliberté, T. Brabec, A. Ruediger, A. J. Carr, A. J. Price, H. S. Gill, L. Ramunno, and F. Légaré, Biomedical Optics Express **5**, 233 (2014).
15. R. M. Williams, W. R. Zipfel, and W. W. Webb, Biophysical Journal **88**, 1377–1386 (2005).
16. S.-W. Chu, S.-P. Tai, M.-C. Chan, C.-K. Sun, I.-C. Hsiao, C.-H. Lin, Y.-C. Chen, and B.-L. Lin, Optics Express **15**, 12,005 (2007).
17. H. C. v. d. Hulst, *Light scattering by small particles* (Dover Publications, New York, 1981). OCLC: 829166958.
18. D. A. D. Parry and A. S. Craig, Biopolymers **16**, 1015–1031 (1977).
19. G. Zhang, Y. Ezura, I. Chervoneva, P. S. Robinson, D. P. Beason, E. T. Carine, L. J. Soslowsky, R. V. Iozzo, and D. E. Birk, Journal of Cellular Biochemistry **98**, 1436–1449 (2006).